Journal of the European Ceramic Society **18** (1998) 1645–1654

PII: S0955-2219(98)00111-3
0955-2219/98/$—see front matter

Detection of Prefracture Microcracking in Al_2O_3 by Acoustic Emission

Patricie Merkert,[a] Mark Hoffman[ab] and Jürgen Rödel[a]*

[a]Department of Materials Science, Ceramics Group Technical University Darmstadt, Darmstadt, Germany
[b]School of Materials Science and Engineering The University of New South Wales, Sydney, Australia

(Received 12 September 1997; accepted 6 April 1998)

Abstract

Acoustic emission monitoring is used to detect prefracture microcracking in alumina of grain sizes ranging from 0·8–9·2 μm. Fracture in samples containing artificial spherical pores of 80 μm diameter was compared with fracture from natural defects. Prefracture microcracking was detected in all samples confirming that fracture in alumina is a two stage process consisting of microcrack nucleation, adjacent to a pre-existing defect, followed by crack propagation to failure. Prefracture microcracking was less prevalent and exhibited lower amplitude acoustic emission signals as grain size decreased. An exception was submicron grain sized alumina which revealed a relatively large number of high amplitude acoustic emissions. This is attributed to a change in fracture initiation mode. © *1998 Elsevier Science Limited. All rights reserved*

Zusammenfassung

Akustische Emissionsmessung wird benutzt, um Mikrorisse vor dem Bruch in Aluminiumoxid mit Korngrößen von 0·8–9·2 μm zu detektieren. Der Bruchvorgang in Proben mit künstlichen sphärischen Poren mit einem Durchmesser von 80 μm wurde mit dem in Proben mit natürlichen Defekten verglichen. Es wurden vor dem Bruch in allen Proben Mikrorisse detektiert, wodurch bestätigt wird, daß der Bruchvorgang in Aluminiumoxid ein Zwei-Stufenprozeß ist, der aus der Mikrorißinitiierung neben einem bereits existierenden Defekt gefolgt von Rißfortschritt bis zum Versagen besteht. Mit abnehmender Korngröße waren Mikrorisse vor dem Bruch weniger vorherrschend und das akustische Emissionssignal besaß geringere Amplituden. Eine Ausnahme war das Aluminiumoxid mit einer Korngröße im Submikronbereich, das eine relativ große Anzahl von akustischen Signalen mit einer hohen Amplitude aufzeigte. Dies wird auf eine Änderung des Bruchinitiierungsmodus zurückgeführt.

1 Introduction

Fracture analysis of engineering materials is usually divided into two fields: crack initiation and crack propagation. In the field of structural ceramics a significant amount of work has been concentrated on the field of crack propagation, notably in the areas of crack growth resistance toughening[1,2] and static[3,4] and cyclic fatigue.[5,6] In comparison, studies of fracture initiation in ceramics are difficult to find. Recent work has proposed that crack extension toughening processes have limited influence upon the fracture strength of structural ceramics[7,8] with the corollary that it is fracture initiation processes that control strength. It is the purpose of this work to investigate the factors affecting fracture initiation in structural ceramics, considering specifically the case of polycrystalline alumina.

Residual stresses form in polycrystalline alumina on cooling following sintering as a result of thermal expansion anisotropy. It has been shown experimentally that these stresses increase from 100–300 MPa as grain size increases from 2–16 μm.[9] Should a load be applied to the sample, localised residual stresses combine with applied stresses resulting in variations in localised stresses. Lawn considered this in developing a model for microcracking in polycrystalline alumina.[10] Here, penny shaped microcracks, of grain size dimensions, are initiated in terms of a microcracking stress intensity factor, K^M:

$$K^M = 2(\sigma_{ii} + \sigma_R)\sqrt{\frac{c_0}{\pi}} \quad (1)$$

where σ_{ii} is the applied stress, σ_R the residual stress and c_0 the prospective crack length. It was predicted that the microcrack would grow to

*To whom correspondence should be addressed.

3–5 times the grain size after which the residual stresses in the crack region are released and equalise to zero.

Fracture may be addressed as a *two stage process*: firstly, applied stresses, locally concentrated by a pre-existing defect, combine with residual stresses to form, or *nucleate*, a microcrack. This stage relieves the residual stress locally. The second stage involves a further increase in applied stress up to a level at which critical crack *propagation* and fracture occurs. As considered recently in other works, defects in a material do not constitute critical flaws but rather are stress concentration sites.[7,11]

In addressing this issue, artificial pores were introduced into alumina to overcome the difficulty of varying size and shape of stress concentration sites. By considering the fracture stress and intrinsic toughness of the material, it was found that fracture causing microcracks, initiating from these artificial pores, were inevitably of twice the average grain size, *independent* of the average grain size.[7,11] The conclusion made was that statistically present exceptionally large grains cause large localised residual stresses, catalysing microcracks on the application of concentrated applied stress. These microcracks relieve the residual stresses but constitute a critical flaw on the application of further applied load.

Based upon the theory that residual stresses result in microcracking it has been found in alumina that at grain sizes above 35–100 μm microcracking occurs spontaneously upon cooling.[1,12,13] As confirmation of this, the formation of microcracks during cooling as a result of thermal expansion anisotropy has been shown by the detection of AE activity, not only in alumina as it is cooled from 400–200°C,[14] but also in Nb_2O_5 on cooling from 450–300°C[15] and porcelain.[16]

Acoustic emission (AE) monitoring provides the possibility to detect microcracking in alumina during mechanical loading but prior to fracture. The formation of a microcrack during loading releases energy in the form of an acoustic wave[17] which propagates through the sample and may be detected using piezoelectric sensors attached to the sample.

Investigations of microcracking during mechanical loading of ceramics by AE detection are limited, but convincing as to the applicability of the technique.[18–20] All authors acknowledge that some difficulties arise from the low energy emission associated with microcrack formation relative to other AE sources present during such testing. Okuno *et al.*[18] first presented data of AE activity during the loading of alumina samples in four point bending. Wakayama *et al.*[19] then refined this process using 5 and 20 μm grain sized alumina samples and Si_3N_4 with 9, 5 and 2·5 μm grain size.[20] In the latter two works, it was found that as load was monotonically increased acoustic emissions were detected and attributed to prefracture microcracking. Microcracking occurred in two stages: (i) nucleation, where the level of AE activity was low, followed by (ii) microcrack coalescence signified by a higher level of AE activity which ended at sample fracture. It was found that the stress for microcrack coalescence decreased with grain size in the Si_3N_4 samples but was independent of grain size in the alumina. The nucleation stress was the same for the two larger grain sized Si_3N_4 samples and not considered in the case of alumina. At grain sizes less than 5 μm detection of characterisable AE activity was unattainable. The small range of grain sizes considered, two in each case, makes conclusions associated with grain size difficult to make.

Kim *et al.*,[21,22] in a further refinement, have modelled the fracture process in alumina samples of different grain sizes based upon the idea of microcrack nucleation catalysed by residual stresses. Prefracture AE activity, attributed to microcracking, was also predicted as a function of increasing applied stress and compared with experimental data. Again only two grain sizes were considered, however, the stress at which AE activity occurs was found to increase with decreasing grain size and/or increasing grain boundary toughness. The clear distinction between microcrack nucleation and coalescence shown by Wakayama[19,20] was not found.

In this work we consider the processes associated with microcrack nucleation and subsequent fracture in alumina. Microcrack nucleation is detected via AE detection with the assistance of an AE signal analysis system which enables characterisation of AE signals specific to microcracking and, hence, the discrimination of low energy microcracking signals. Four different grain sized materials are considered to provide a variation in residual stresses and microcrack size. As fracture inevitably initiates from a source of stress concentration within the sample, spherical pores are artificially introduced into the material to provide a stress concentration site of constant shape and dimension. Results are then compared with those obtained from samples, without artificially introduced defects, where fracture initiates from natural defects in the same material.

2 Experimental Procedure

2.1 Sample preparation and mechanical testing

Alumina samples were produced by slip casting using a process which is explained in more detail

elsewhere.[7] Briefly, billets were produced by mixing commercial ultrafine alumina powder with an average grain size of 0·2 μm (TM-DAR, Taimei Chemicals) with 2 wt% binder (Carbowax PEG-8000) at a pH-value of 3·8. $Mg(NO_3)_2 \cdot 6H_2O$ was added to introduce 1000 ppm MgO to hinder anisotropic grain growth[23] during sintering. It is estimated that about half of this MgO is lost during slip casting with the remaining MgO being only slightly above the solid solution limit at the sintering temperature. This amount of MgO doping was chosen to yield a sufficient dopant level to assure formation of an equiaxed grain structure while forming only a negligible amount of second phase spinel. Elsewhere,* using the same slip chemistry, 0·025 vol% polystyrene spheres (100 μm diameter) were added to the slip in producing some of the billets. All billets were sintered to a density of 98–99% in an alumina powder bed containing 1000 ppm MgO at 1350°C for 30 min. During sintering, the polystyrene spheres were burnt out resulting in spherical pores of approximately 80 μm diameter. To produce three additional grain sizes coarsening steps were undertaken at 1600°C for 0·5, 3 h and 12 h. Bend bars ($30 \times 4 \times 3\,mm^3$) were cut from the billets. All faces and the ends were ground and the tensile face polished to a 1 μm finish and the edges chamfered. Five bars with artificial pores and twenty without were produced for each of the four different grain sizes.

The bend bars were then tested in a servohydraulic test machine (MTS 810) in four-point bending with an inner/outer span of 10/20 mm and a loading rate of $100\,N\,s^{-1}$.

2.2 Acoustic emission detection

2.2.1 Background

When a microcrack forms in a sample some of the energy released is converted into an acoustic wave which propagates through the sample.[17,24] This wave may be detected using piezoelectric AE sensors. The form of the acoustic wave varies according to its source, sample geometry and material, internal reflections and the source–sensor distance. The sensor then superimposes its own characteristics such as damping behaviour and carrier frequencies on the detected wave. Figure 1 shows, schematically, a typical acoustic emission (AE) signal. To register as an AE, a signal must have an amplitude above a specified threshold. The time span with amplitudes above this threshold is termed the duration time, t_D, and the time from the first above threshold peak to the maximum detected peak, the rise time, t_R. The total acoustic energy is calculated by integrating over the squared amplitude during the duration time. Energy, t_R and t_D are traditionally used to characterise AEs.

2.2.2 Testing

Figure 2 shows a schematic representation of the experimental set-up used to detect AEs during loading in four-point bending. Wide band (300–1000 kHz) sensors (Physical Acoustics Corp., Pico type, modified as differential sensor) were attached to each end of the bend bar using a low viscosity couplant (Silicon oil AK 350 Wacker) and held in place with a rubber band looped around the back of the sensors and passed along the length of the sample. Detected signals were transferred from the sensor through a preamplifier, with variable gain of 45–60 dB, to a PC operated AE detector unit (AMS3 from Vallen Systems, Germany). The signal is then further amplified, digitised and analysed to determine the characteristic rise time, energy, duration and amplitude of each wave. For the testing undertaken in this work preamplifier gain was set at 60 dB with a detected signal threshold level of 0·028 μV. Prior to testing the acoustic wave velocity in each sample was determined by actively

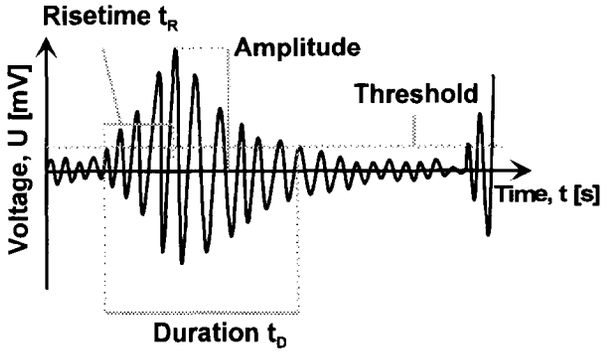

Fig. 1. Schematic representation of an AE signal as detected by a piezoelectric sensor. Output voltage, U, is plotted versus time, t and characteristic features indicated.

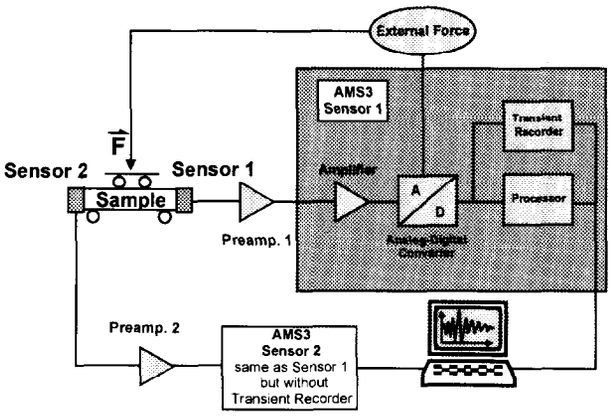

Fig. 2. Schematic representation of experimental configuration for detecting and analysing AE signals during loading in four-point bending.

*See acknowledgements.

pulsing one sensor, detecting the pulse with other sensor and measuring time between pulse emission and detection, i.e. the travel time along the sample. The process was repeated in both directions. Using the wave velocity and the difference between the arrival time of AE signals for a particular AE event (microcrack, friction etc.) at each of the sensors, the location of the event could be determined. The accuracy of this process was however limited to ± 1 mm due to the sampling rate of the A/D converter which caused an error in the wave velocity measurement.

The applied load was continuously monitored from the test machine controller and each time an AE signal rose above the threshold amplitude its arrival time, wave characteristics, location and the applied load were recorded on the PC.

A transient recorder was attached to one of the sensors which recorded the wave form of each above threshold AE signal on the PC. Following testing the signal was analysed using fast Fourier transformation software. Only the rising part of the signal was analysed because essential information about the AE-source is found in the first peak of the AE signal.[25,26] Due to the short rise time of the signals a time window of 6 μs was taken, being the smallest available with the software used and representing 32 points with a recording frequency of 5 MHz. Some background noise was inevitably included in this analysis, nevertheless, clear signal characterisation was possible in most cases.

Prefracture microcracking is not the only possible source of AEs during this type of testing. Friction from the four-point bend rollers and test machine as well as electromagnetic noise may register as above threshold AEs, especially given the low energy of signals resulting from microcracking. While individual signal analysis may be used to distinguish microcracking AE events from others, removing unwanted signals altogether is far more attractive given the time required to individually analyse each signal; to reduce AEs as a result of roller contact it was found that the application of Scotch® tape prior to each test was quite effective, the bend bars were given a length of 30 mm to reduce interference between the outer rollers and the sensors, to reduce electromagnetic noise a Faraday cage was built around the sample, sensors and four-point bend device and a 0·1–300 MHz wide band filter placed between the power supply and the AE analyser.

Following mechanical testing and AE signal analysis the fracture surface of all samples which produced AEs attributive to microcracks were investigated in a scanning electron microscope (SEM) to determine the fracture origin.

3 Experimental Results

Microstructures with equiaxed grain morphology were obtained as seen in Fig. 3. Grain sizes were determined using the linear intercept method over at least 300 intersections and are shown in Table 1.

Acoustic wave velocity was measured to be 6000 m s^{-1} in all alumina samples and is in the region of that quoted in other work.[18,19]

Signals attributable to microcracking or friction were discriminated. Taking a sample which fractured between the inner rollers of the four-point bend fixture and at a distance of more than 1 mm from both rollers, such as shown in Fig. 4, it may be assumed that prefracture AE signals on the fracture plane represent microcracking and signals near the rollers represent friction or some form of event associated with roller-sample contact. No consistent difference could be ascertained between the rise time, duration, energy or amplitude of signals located at these two sources. However, frequency analysis of these signals revealed two distinct mutually exclusive analyses which are deemed to be characteristic of an acoustic emission of a microcrack and a roller contact event. A typical signal shape and frequency analysis for microcrack and roller signals are shown in Fig. 5(a) and (b), respectively. Specifically, microcrack signals show a single maximum at 500 kHz while roller contact signals show two peaks at 100–200 kHz and 500 kHz. This information proved useful to distinguish the source of AE signals where the fracture plane was close to the rollers and signal source location could not be used to distinguish AE events associated with prefracture microcracking from roller-sample contact. Only signals located on a fracture plane near the inner rollers were analysed in this way.

Not all AE signals located on fracture planes < 1 mm from the inner rollers could be evaluated as either microcracks or contact signals. In the cases where signal analysis was used, i.e. when the

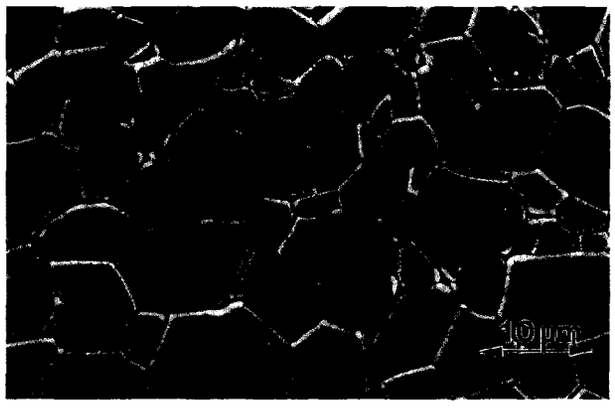

Fig. 3. Sample SEM micrograph of 8·5 μm grain size material following thermal etching showing equiaxed grain morphology.

Table 1. Grain coarsening time, average grain size and number of AE signals detected prior to fracture and characterisable as microcracks for all materials tested

	Average grain size (μm)		*No. of samples with AE signals characterisable as microcracks and average no. of signals per sample in parentheses*	
Coarsening time at 1600°C (h)[a]	*80 μm artificial pores*	*No artificial pores*	*80 μm artificial pores—from 5*	*No artificial pores—from 20*
0	0·8	0·8	4 (3)	11 (4·6)
0.5	3.4	4.4	2 (1)	8 (1.5)
3	5.5	6.1	1 (1)	11 (2.9)
12	9.2	8.5	5 (2)	10 (3.6)

fracture plane was < 1 mm from the rollers, 35% of the signals could be distinguished as microcracks, 20% as roller contact signals and 45% could not be distinguished as either. Significantly, at least half of the indistinguishable events recorded a time difference between detection at each of the two sensors of greater than the travel time from one end of the sample to the other and, hence, were deemed to be errors in the system calculation.

Signals outside the span of the inner rollers, taking into account the localisation error of the system, were not considered. Signals within the inner span, but not on the fracture plane, as seen in Fig. 4, were not analysed but generally occurred at stresses higher than the first detected event and may represent microcracks that do not evolve into a critical flaw. In cases where no AE signals occurred which could be clearly attributed to microcracks the sample was rejected. Table 1 shows the number of samples where AE signals could be clearly characterised to be the result of prefracture microcracking.

As a sample was monotonically loaded the first AE signal heard which could be attributed to microcracking and which was located on the subsequent fracture plane was deemed to represent the nucleation of the critical microcrack. The stress at which it occurred is defined as the critical microcracking stress, σ_c. The first detected microcrack was almost invariably on the fracture plane.

The fracture stress, σ_f, and microcracking stress, σ_c, are shown as a function of grain size in Fig. 6(a) and (b) for samples with and without artificial flaws, respectively. Surprisingly, the fracture stress is lower for the samples without artificial flaws

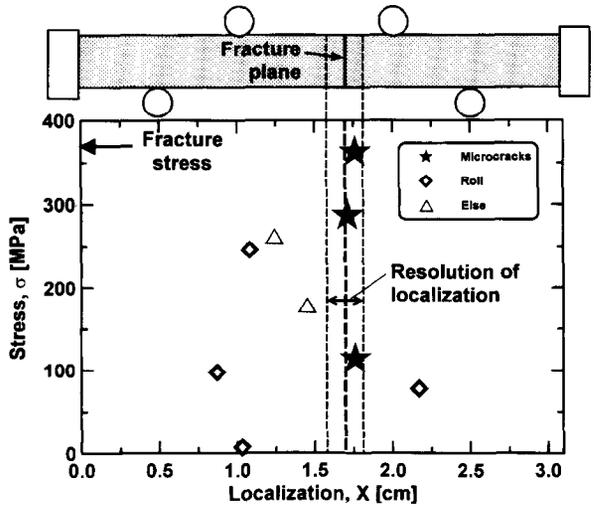

Fig. 4. Sample plot of AE event location, X versus applied stress, σ. Shown are the AE events attributed to microcracking on the fracture plane, roller-sample contact and undetermined signals located away from either of these sources.

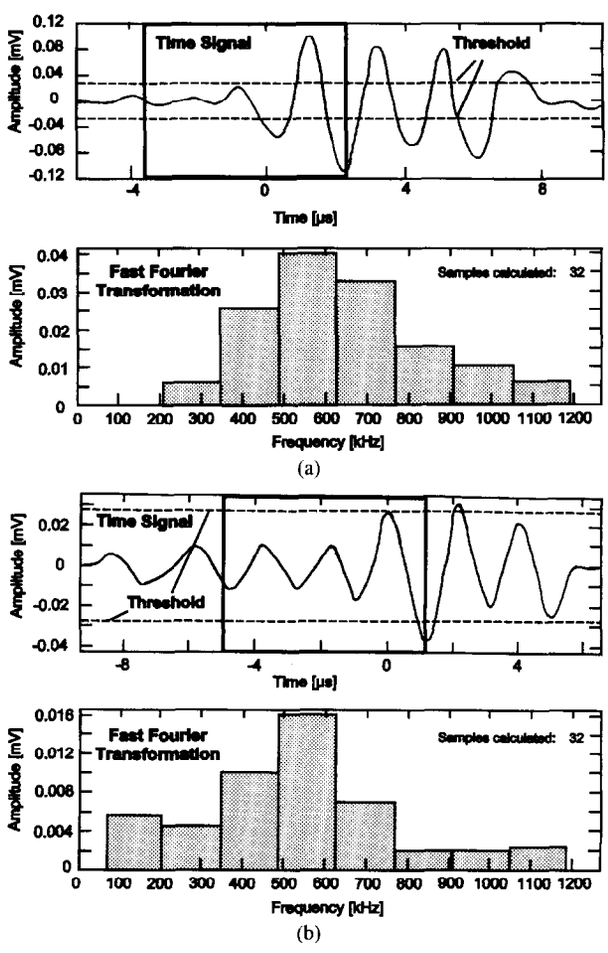

Fig. 5. Sample plots of a detected AE signal plotted as voltage, U, versus time, t, and the corresponding frequency analysis using fast Fourier transformation for signals attributed to (a) microcrack nucleation and (b) roller-sample contact.

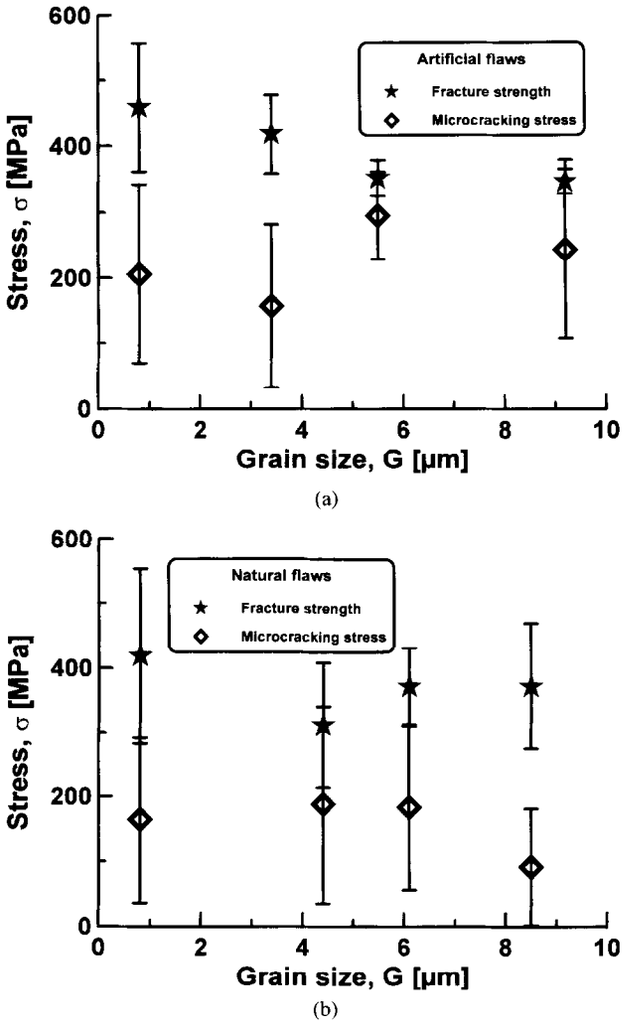

Fig. 6. Critical microcracking stress, σ_c, and fracture stress, σ_f, plotted versus grain size, G, for samples (a) with and (b) without artificially introduced defects.

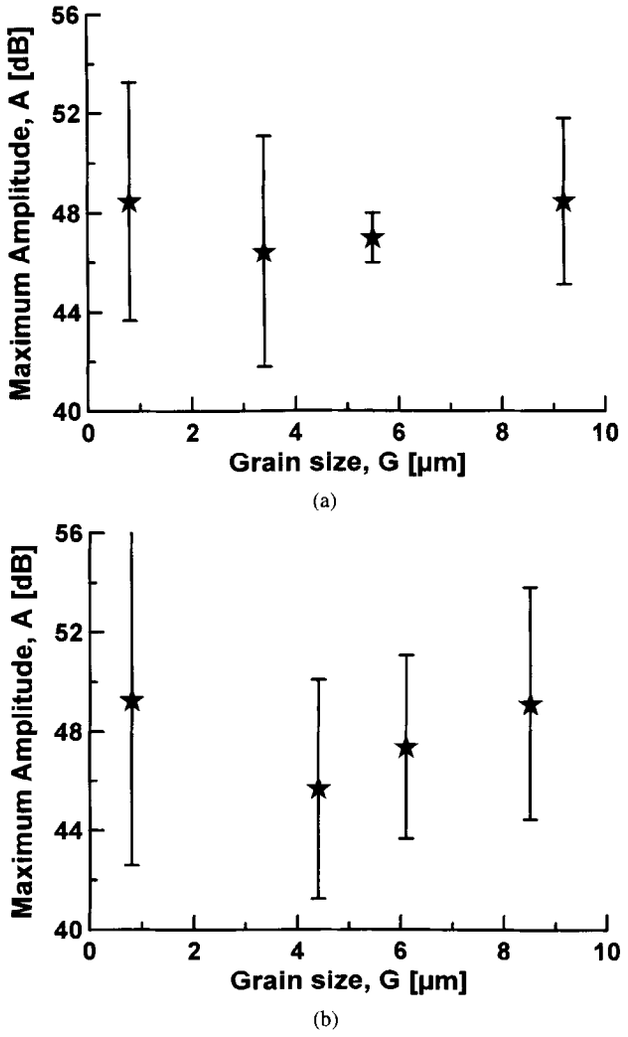

Fig. 7. Maximum amplitude, A, of signals attributed to microcracking versus grain size, G, for samples (a) with and (b) without artificially introduced defects.

than those containing them. This is believed attributable to the samples being produced in separate laboratories. The fracture strength of samples without artificial flaws was significantly higher in similar samples produced in that same laboratory.[7] Nevertheless, the mechanisms being studied in this work are not compromised. Large standard deviations exist for the microcracking stress in both cases. This is not unexpected, given that the maximum residual stress, which is believed to influence the microcracking stress, results from the random orientation of grains and is therefore, itself a semi-random quantity. The standard deviations in the fracture strength are less for the samples containing artificial flaws. This is a consequence of the fact that in this case the stress concentrating defects, which evolve to be fracture origins, are of a constant size and shape, whereas, naturally occurring defects are of a variable size and shape and therefore concentrate the stress to varying degrees.

Fig. 7(a) and (b) show the maximum amplitude of AE signals attributed to microcracking as a function of grain size for samples with and without artificial flaws. The average maximum amplitude of these signals increases with grain size, with the exception of the submicron grain sized material which will be considered later. The amplitude as a function of grain size is independent of whether fracture originates from an artificial or natural defect. Both of these features are consistent with the hypothesis that microcracks scale with the grain size as the larger the microcrack the greater the energy associated with its nucleation and subsequent AE signal. Table 1 shows that the number of detected microcracks, and the average number of signals (or counts) per sample, also increases with grain size, again with the exception of the submicron grain sized material. It is possible that signal amplitude and the number of detected microcracks are directly related i.e. that the larger the grain size the greater the number of AEs which will lie above the detection threshold. Analysis, shown later, indicates, however, that this is not necessarily the case.

Figure 8(a)–(c) shows the three types of fracture origins identified in this study. Figure 8(a) shows an artificial pore located close to the tensile surface, typical of all samples containing these defects. Figure 8(b) shows a pore occurring naturally as a result of processing and is typical of the fracture origins found in the samples, without artificially introduced flaws, with an average grain size $\geq 3{\cdot}4\,\mu m$. Figure 8(c) shows a surface defect resulting from sample handling, grinding or polishing. This type of fracture origin is characteristically found on the fracture surface of the submicron grain sized samples not containing artificially inserted defects.

(a)

(b)

(c)

Fig. 8. Fracture origins in alumina: (a) artificially introduced spherical pore, (b) natural processing pore and (c) sample preparation defect.

4 Discussion

In another work it was proposed that processing defects concentrate applied stress within the bulk of a sample. Fracture was then calculated to occur from a microcrack, adjacent to this defect, of approximately two average grain diameters in size.[7] The effects of crack growth resistance toughening have been found to be insignificant in determining the fracture strength of alumina with critical defects of grain sized dimensions.[7,8] The question is then posed as to what is the nucleation process of these microcracks. A further work proposed that these microcracks formed at pre-fracture stresses, as a consequence of inherent residual stresses, resulting in a two step fracture process:[11] crack *nucleation*, followed by *propagation* to fracture. The determination of prefracture microcracking via AE detection in this work provides strong evidence supporting this hypothesis.

The formation of a microcrack causes the localised residual stresses, which catalyse its formation, to be relieved. Rearranging eqn (1):

$$\sigma_{c,f} = \frac{K^M}{2}\sqrt{\frac{\pi}{c_0}} - \sigma_R \qquad (2)$$

Therefore, prior to microcracking σ_R is significant and eqn (2) gives the critical microcracking stress, σ_c, or stress for crack *nucleation*. Following microcracking the local residual stresses are relieved, σ_R becomes equal to zero and eqn (2) gives the fracture stress, σ_f: the stress for crack *propagation*. A ratio of the critical microcracking stress to fracture stress, σ_c/σ_f, can then be calculated.

By taking K^M to be the intrinsic toughness of alumina, $\sim 2\,MPa\sqrt{m}$,[27] and c_0 to be twice the average grain size and the size of a critical microcrack,[7] one

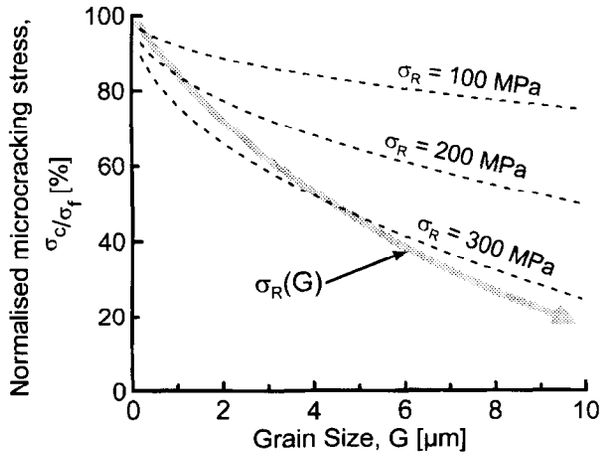

Fig. 9. Predicted critical microcracking stress, σ_c, normalised with fracture stress, σ_f, plotted versus grain size, G, for typical levels of residual stress, σ_R. Shown also is a hypothetical curve for residual stress increase with grain size.

may determine σ_c/σ_f as a function of grain size for various residual stress values. This is shown in Fig. 9 for typical residual stresses ranging from 100–300 MPa.[9] It can be seen that as grain size increases the relative value of stress at which microcracking occurs decreases. Additionally, it should be remembered that the residual stress has been shown to increase with increasing grain size[9] and therefore the relative microcracking stress will decrease even more dramatically with increasing grain size. This is shown hypothetically in Fig. 9 as the curve $\sigma_R(G)$ which will intersect $\sigma_c/\sigma_f = 100\%$ at $G = 0$ and the x-axis, $\sigma_c/\sigma_f = 0\%$, at the critical grain size for spontaneous microcracking.

The above analysis ignores the stress concentrating effects associated with inherent defects by assuming an embedded penny shaped flaw and therefore, a quantitative comparison with experimental values cannot be made. However, qualitative comparison may be obtained. Figure 10(a) and (b) shows the measured microcracking stress normalised with the fracture stress, $\sigma c/\sigma_f$, as a function of grain size for samples with and without artificial flaws. In the samples without artificial flaws [Fig. 7(b)], with the exception of the submicron grain sized samples, there is a clear decrease in σ_c/σ_f as a function of grain size, as predicted. The large error bars are caused by the addition of the standard deviations of the fracture and microcracking stress data shown in Fig. 6. Such a clear pattern cannot be seen in the samples containing artificial flaws [Fig. 7(a)] though it should be noted that these data represent, statistically, a much smaller data set (Table 1) than the samples without artificial flaws.

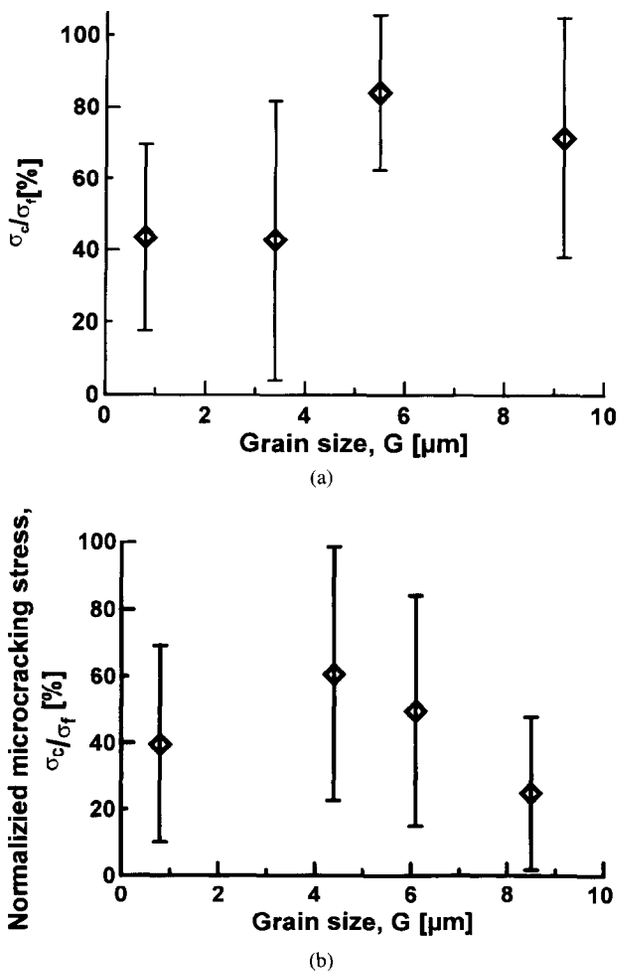

Fig. 10. Critical microcracking stress, σ_c, normalised with fracture stress, σ_f, plotted versus grain size, G, for samples (a) with and (b) without artificially introduced defects.

The submicron grain sized material shows exceptions to the grain size dependence patterns of the larger grain sized materials when amplitude and σ_c/σ_f are plotted against grain size. The reason for this can be found in the fracture surface analysis. In the case where the grain size is $\geq 3{\cdot}4\,\mu$m, specimen fracture usually originates from processing defects, be they artificially introduced [Fig. 8(a)] or naturally occurring [Fig. 8(b)]. Microcracks then form as a result of concentration of the applied stress in these regions combined with residual stresses. Fracture origins in the submicron grain sized material were usually determined to be cracks near the tensile surface [Fig. 8(c)]. These microcracks, which are significantly larger than the grain size, are introduced into the material during sample preparation. Another form of stress concentration therefore occurs during load application which results in cracking at lower applied stresses relative to the larger grain sized materials. In another, previously mentioned work,[7] it was found that critical microcracks in submicron grain sized alumina were significantly larger than two average grain diameters, as found with larger grain sized materials. This then provides an explanation for the larger than expected maximum AE amplitudes detected in the submicron grain sized material prior to fracture (Fig. 7).

Residual stresses vary throughout the bulk of the material. Hence, an increase in the maximum residual stress with grain size represents, additionally, an increase in the range of residual stresses within the sample. A larger grain sized sample, therefore, will not only exhibit initial prefracture microcracking at a relatively low stress but will exhibit far more prefracture microcracking over a wider range of applied stresses. This is shown by the increase, with grain size, in the average number of AE signals detected per sample displayed in Table 1.

5 Conclusions

Acoustic emission monitoring was undertaken during monotonic loading to fracture of alumina

of grain size 0·8–9·2 μm with natural and artificially induced spherical flaws (diameter 80 μm);

1. Acoustic emission signals were detected at prefracture stresses for all types of samples. Analysis enables certain signals to be attributed to prefracture microcracking in the material.
2. Fracture in alumina is a two stage process: (i) nucleation of microcracks catalysed by the presence of thermal anisotropic residual stresses, followed by (ii) crack propagation to failure.
3. The maximum amplitude of prefracture AE signals, caused by microcracking, increases with grain size indicating that the size of prefracture microcracks scales with the grain size.
4. The critical stress for microcracking and the fracture stress appear to decrease with grain size. Application of a simple model shows that the decrease in microcracking stress is influenced by increasing residual stress with grain size and cannot be explained simply by increasing microcrack size.
5. Defects within the sample lead to stress concentrations which constitute fracture origins. In submicron grain sized samples these defects occur on the surface and are formed during sample preparation. In larger grain sized samples critical defects exist inherently in the microstructure and are formed during processing.

Acknowledgements

Sincere thanks are given to André Zimmermann who kindly provided us with the alumina samples containing artificial pores and for helpful discussions. Also to Dr Doru Lupascu for helpful discussions and for critically reviewing the manuscript. Financial support was provided by the German Research Association under contract no. Ro 954/6-1.

References

1. Chantikul, P., Bennison, S. J. and Lawn, B. R., Role of grain size in the strength and r-curve properties of alumina. *Journal of Am. Ceram. Soc.*, 1990, **73**(8), 2419–2427.
2. Becher, P. F., Microstructural design of toughened ceramics. *Journal of Am. Ceram. Soc.*, 1991, **74**(2), 255–269.
3. Fett, T. and Munz, D., Subcritical crack growth of macrocracks in alumina with r-curve behavior. *Journal of Am. Ceram. Soc.*, 1992, **75**(4), 958–963.
4. Jensen, D. G., Zelizko, V. and Swain, M. V., Small flaw static fatigue crack growth in Mg-PSZ. *Journal of Mat. Sci. Lett.*, 1989, **8**, 1154–1157.
5. Lathabai, S., Rödel, J. and Lawn, B. R., Cyclic fatigue from frictional degradation at bridging grains in alumina. *Journal of Am. Ceram. Soc.*, 1991, **74**(6), 1340–1348.
6. Hoffman, M., Mai, Y. -W., Wakayama, S., Kawahara, M. and Kishi, T., Crack-tip degradation processes observed during in-situ cyclic fatigue of partially stabilised zirconia. *Journal of Am. Ceram. Soc.*, 1995, **78**(10), 2801–2810.
7. Zimmermann, A., Hoffman, M., Flinn, B. D., Bordia, R. K., Chuang, T.-J., Fuller, Jr, E. R. and Rödel, J., Fracture of alumina with controlled pores. *Journal of Am. Ceram. Soc.*, in press.
8. Seidel, J., Claussen, N. and Rödel, J., Reliability of alumina ceramics I: effect of grain size. *Journal of European Ceramic Society*, 1995, **15**, 395–404.
9. Ma, Q. and Clarke, D. R., Piezospectroscopic determination of residual stresses in polcrystalline alumina. *Journal of Am. Ceram. Soc.*, 1994, **77**(2), 298–302.
10. Lawn, B. R., Fundamental condition for existence of microcrack clouds in monophase ceramics. *Journal of European Ceramic Society*, 1991, **7**, 17–20.
11. Hoffman, M. and Rödel, J., Suggestion for mechanism of strengthening of nanotoughened ceramics. *Journal of Ceram. Soc. Jpn.*, 1997, **105**(12), 1086–1090.
12. Rice, R. W. and Pohanka, R. C., Grain-size dependence of spontaneous cracking in ceramics. *Journal of Am. Ceram. Soc.*, 1979, **2**(11-12), 559–563.
13. Clarke, D. R., Microfracture in brittle solids resulting from anisotropic shape changes. *Acta Metall.*, 1980, **28**, 913–924.
14. Breval, E., Srikanth, V. and Subbarao, E. C., Acoustic emission and microcracking in sapphire, sintered Al_2O_3, Al/Al_2O_3 composite, and aluminum. *Journal of Am. Ceram. Soc.*, 1995, **78**(9), 2541–2544.
15. Srikanth, V. and Subbarao, E. C., Thermal expansion anisotropy, microcracking and acoustic emission of Nb_2O_5 ceramics. *Ceram. Intern.*, 1992, **18**, 251–261.
16. Kirchhoff, G., Pompe, W. and Bahr, H.-A., Structure dependence of thermally induced microcracking in porcelain studied by acoustic emission. *Journal of Mat. Sc.*, 1982, **17**, 2809–2816.
17. Steeb, S. and 12 Mitautoren, Zerstörungsfreie Werkstück- und Werkstoffprüfung. Staib, W., Chapter 11 Schallemissionsverfahren. Expert verlag, Ehningen bei Böblingen, 1988, S. 465–489.
18. Okuno, A., Shiwa, M. and Kishi, T., AE analysis of fracture mechanisms of beta-alumina during four-point bending test. *Journal of Ceram. Soc. Jap.*, 1990, **98**(1), 103–108.
19. Wakayama, S. and Nishimura, H., Critical stress of microcracking in alumina evaluated by acoustic emission. *Fract. Mech. Ceram.*, 1992, **10**, 59–72.
20. Wakayama, S., Iwata, M. and Kawahara, M., AE studies on the microfracture process in silicon nitride. *Progress in Acoustic Emission VI*, 1992, 551–558.
21. Kim, B.-N., Naitoh, H., Wakayama, S. and Kawahara, M., Simulation of microfracture process and fracture strength in 2-dimensional polycrystalline materials. *JSME International Journal*, 1996, **39**(4), 548–554.
22. Kim, B.-N., Naitoh, H. and Wakayama, S., Simulation of AE generation behavior in 2-dimensional polycrystals by using the body force method. *JSME International Journal*, 1996, **39**(4), 633–639.
23. Rödel, J. and Glaeser, A. M., Anisotropie of grain growth in alumina. *Journal of Am. Ceram. Soc.*, 1990, **73**(11), 3292–3301.
24. Beattie, A. G., Acoustic emission, principles and instrumentation. *Journal of Acoustic Emission*, 1983, **2**(1/2), 95–128.
25. Obata, Y., Yasunaka, T., Mori, Y., Aoki, K. and Tsune, M., Acoustic emission waveform analysis during fatigue crack propagation in SUS304 steel at room temperature. *Progress in Acoustic Emission II*, 1984, 255–261.

26. Sklarczyk, C., Schallemissionanalyse der Bruchvorgänge in Al_2O_3-Keramik. DFG-Abschlußkolloquim: Mikrobruchvorgänge in Al_2O_3-Keramiken, 1990, 150–174.

27. Seidel, J. and Rödel, J., Measurement of crack tip toughness in alumina as a function of grain size. *Journal of Am. Ceram. Soc.*, 1997, **80**(2), 433–438.